Life Sciences 224 (2019) 12–22

Contents lists available at ScienceDirect

Life Sciences

journal homepage: www.elsevier.com/locate/lifescie

MiR-451 antagonist protects against cardiac fibrosis in streptozotocin-induced diabetic mouse heart

Cui Liang, Lu Gao, Yuan Liu, Yuzhou Liu, Rui Yao, Yapeng Li, Lili Xiao, Leiming Wu, Binbin Du, Zhen Huang, Yanzhou Zhang*

Department of Cardiology, The First Affiliated Hospital of Zhengzhou University, Zhengzhou, China

ARTICLE INFO

Keywords:
miR-451
Diabetic cardiomyopathy
Endothelial-mesenchymal transition
AMPKa1

ABSTRACT

Aims: MicroRNAs (miRNAs or miRs) are a large class of small noncoding RNAs. The present study aims to evaluate the effect of miR-451 on cardiac remodeling in diabetic cardiomyopathy.

Main methods: Mice were injected with streptozotocin (STZ) to induce diabetes. Twelve weeks after final STZ injection, mice were subjected to myocardial injection of adenovirus (Ad)-shmiR-451 to knock down miR-451. Mouse heart endothelial cells (MHECs) were treated with a miR-451 antagomir to inhibit miR451 and were exposed to high glucose.

Key findings: Sixteen weeks after STZ injection, mice exhibited no significant cardiac hypertrophy but did exhibit serious cardiac fibrosis. MiR-451 knockdown attenuated cardiac fibrosis and improved cardiac function. Moreover, we found that miR-451 knockdown suppressed endothelial-to-mesenchymal transition (EndMT) in diabetic mouse hearts. Hyperglycemia-induced EndMT in MHECs was attenuated by the miR-451 antagomir. Activation of AMPKa1/mTOR was decreased in diabetic mouse heart tissue and hyperglycemia-stimulated MHECs, which was increased following miR-451 knockdown or inhibition. AMPKa1 siRNA abrogated the anti-EndMT effects of miR-451 knockdown in MHECs.

Significance: miR-451 participates in the pathology of diabetic cardiomyopathy via AMPKa1-regulated EndMT in endothelial cells.

1. Introduction

Cardiac fibrosis is a significant feature of diabetic cardiomyopathy in both diabetes patients and animal models [1]. In diabetic cardiomyopathy (DCM), extracellular matrix protein deposition and matrix cross-linking increase myocardial stiffness, which mediates cardiac diastolic dysfunction [2]. Myocardial fibrosis plays an important role in the pathogenesis of diabetes-related heart failure. In diabetes cardiomyopathy, cardiomyocyte hypertrophy and microvascular abnormalities are often accompanied with cardiac fibrosis [3]. Endothelial cells (ECs) are the initial targets of hyperglycemia during the pathological process of diabetes. EC injury plays an important role in extracellular matrix (ECM) secretion and promotes the development of chronic diabetic complications [4,5]. ECs undergo endothelial-to-mesenchymal transition (EndMT) after sustained damage. In this transdifferentiation process, ECs lose cellular markers such as vascular endothelial (VE)-cadherin and CD31, and obtain mesenchymal characteristics, such as vimentin (Vim) and a-smooth muscle actin (SMA) expression [6]. EndMT is involved in the pathology of cardiac fibrosis in both type 1 and type 2 diabetes-induced cardiomyopathy [7,8].

Transforming growth factor beta (TGFβ) is a highly effective protein that is widely distributed during the pathogenesis of cardiac fibrosis [9]. TGF-β1 mediates cardiac fibroblast activation and ECM production, and it preserves a secretory phenotype in cardiac fibroblasts [10]. TGFβ also regulates the EndMT process via suppression of endothelial marker expression [11]. TGFβ/Smad signaling is the most important pathway of EndMT. Once activated, the transcription of key genes related to EndMT is actuated by smad complexes [11]. Targeting of this pathway may be a promising strategy.

MicroRNAs (miRNAs or miRs) are a large class of small noncoding RNAs. miRNAs suppress the translation of target mRNA, depending on the complementarity between the 5′ side seed sequence of the miRNA and the 3′untranslated region (3′ UTR) of the target mRNA [12]. Several reports have indicated that miRNAs are involved in DCM in a type 1 DM model of streptozotocin (STZ)-induced diabetic mice [13,14]. MiR-451 has been reported to participate in many pathological processes, including cancer cell survival and transfer [15–17]. MiR-451 also been found to suppresses the expression of NF-kappaB-mediated

* Corresponding author at: Department of Cardiology, The First Affiliated Hospital of Zhengzhou University, No. 1 Jianshe East Road, Zhengzhou 450052, China.
E-mail address: yzzhang6@163.com (Y. Zhang).

https://doi.org/10.1016/j.lfs.2019.02.059
Received 25 December 2018; Received in revised form 25 February 2019; Accepted 27 February 2019
Available online 11 March 2019
0024-3205/

proinflammatory molecules via LMP7 inhibition in diabetic nephropathy [18]. In cardiovascular disease, miR451 expression decreases in hypertrophic cardiomyopathy patients and regulates cardiac hypertrophy and cardiac autophagy [19]. Yasuhide Kuwabara et al. also reported that miRNA-451 exacerbates lipotoxicity in cardiac myocytes and high-fat diet-induced cardiac hypertrophy [20]. However, the effect of miR-451 on STZ-induced type 1 DCM is unclear. The present study aimed to evaluate the effect of miR-451 on cardiac remodeling in STZ-induced type 1 DCM.

2. Materials and methods

2.1. Materials

AMPKa1 siRNA was purchased from Santa Cruz. The miR-451 antagomir was purchased from Thermo Fisher Scientific.

2.2. Animal models

All of the animal care and experimental procedures conformed to the Guidelines for the Care and Use of Laboratory Animals, published by the United States National Institutes of Health (NIH Publication, revised 2011), Instructional Animal Care and Use Committee (IACUC) and the Guidelines for the Care and Use of Laboratory Animals of the Chinese Animal Welfare Committee, and they were approved by the Animal Use Committees of our hospital and our institute (WDRX-2016K0506). Male C57/B6 mice (8–10 weeks old) were purchased from the Chinese Academy of Medical Sciences (Beijing, China). The mouse diabetes model was established by streptozotocin (STZ) injection, as previously described [21]. Briefly, the DCM model was established by intraperitoneal streptozotocin (STZ) injections (dissolved in 0.1 mol/l citrate buffer, pH 4.5) at a dose of 50 mg/kg for 5 consecutive days. Control mice were injected with equal volumes of citrate buffer. One week after the final STZ injection, fasting blood glucose (FBG) was measured. Diabetes was defined as FBG $\geq$16.6 mmol/l on three independent measurements. Mice for knockdown of miR-451 were subjected to myocardial injection of adenovirus (Ad)-shmiR451 at 12 weeks after diabetes induction since mice developed diabetic cardiomyopathy at 12 weeks of diabetes pathology. Hearts were removed 16 weeks after the final STZ injection.

2.3. Echocardiography and hemodynamics

Mice were anesthetized with 1.5% isoflurane and subjected to echocardiography measurement using a MyLab 30CV ultrasound (Biosound Esaote), as described previously [22,23]. The left ventricular (LV) ejection fraction (LVEF) and LV ejection of shortening (LVFS) were analyzed for > 10 beats per heart.

Mice were anesthetized with 1.5% isoflurane and subjected to hemodynamic measurements using cardiac catheterization, as described previously [22,23]. PVAN data analysis software was used to process the data.

2.4. Histological analyses

H&E, picrosirius red staining, immunohistochemical analysis and immunofluorescence staining were performed according to our previous studies [22,24]. The following antibodies were used for immunohistochemical and immunofluorescence staining: collagen III, CD31, and α-SMA.

2.5. Adenoviral vector construction

2.5.1. Construction of recombinant Adenovirus

Recombinant adenovirus-expressing mouse shmiR451 (Ad-shmiR451) was purchased from Vigene Bioscience Company (Jinan, China). The AMPKa1 siRNA was purchased from Santa Cruz (sc-29,674).

2.5.2. Viral delivery protocol

Mice received myocardial injections of either Ad-shmiR451 or Ad-shRNA (1×10^{10} viral particles (vp) per animal) 12 weeks after the final STZ injection, according to our previous study [21]. Briefly, we chose the left ventricular apex (1 site), anterior wall (2 sites), and lateral wall (2 sites) as injection sites. Each site was injected with 10 μl lentivirus vector (1×10^{10} vp) using a 29-gauge syringe.

2.6. Cell culture and treatment

Primary mouse heart ECs (MHECs) were isolated as described previously [8]. Briefly, mouse hearts were sliced in Hanks' balanced salt solution buffer. Collagenase A was used to digest heart tissue. FBS-DMEM (10%) was used to stop the digestion. The solution was filtered through a nylon mesh (70-mm pores), and cells were resuspended in the Hanks' solution. CD31 beads were used to bind ECs. Beads were washed, and ECs were cultured in dishes precoated with 2% gelatin (Sigma, Oakville, ON, Canada) in endothelial basal medium with 10% FBS at a density of 1×10^5 cells/ml. Cells were cultured in serum-free media for 24 h. MHECs were cultured with 33 mM glucose (high glucose, HG) for 48 h in the presence or absence of miR-451 antagomir. Cells in the control group were exposed to a normal glucose concentration (NG; 5.5 mM glucose) and 27.5 mM mannitol to control for osmolarity. Each experiment was performed three times independently. AMPKa1 siRNA was used to inhibit AMPKa1.

Primary adult rat cardiac fibroblasts were prepared. Briefly, cardiac ventricles from adult male Sprague-Dawley rats (180–220 g) were separated and cut into 1-mm^3 volume pieces. Then, these small pieces were digested in 0.1% collagenase type II for 30 min at 37 °C, followed by 0.25% trypsin for three 5-min periods. The collagenase type II digestion steps were repeated 2–3 times until the tissue was completely digested. The cells were combined, centrifuged, and resuspended in DMEM containing 10% fetal bovine serum for 90 min. Non-adhered cells were removed, and the attached cells were further cultured in a humidified atmosphere of 5% CO2 at 37 °C. Cells from passages 2–4 were used for experiments. CFs were treated with TGFβ1 (10 ng/ml, Sigma) and miR-451 antagomir for 24 h.

2.6.1. Neonatal rat cardiomyocyte (NRCM) culture

One- to 2-day-old Sprague-Dawley rats were sacrificed by cervical dislocation. Hearts were quickly removed, the ventricles washed with PBS three times and incubated with 0.125% trypsin-EDTA (Gibco) for 15 min. Ventricles were then enzymatically digested four times for 15 min each in 0.125% trypsin-EDTA in PBS. Digestion was stopped by the addition of FBS at a final concentration of 10%. The cells were then centrifuged at 250 ×*g* for 8 min and resuspended in DMEM/F12 (Gibco) supplemented with 10% FBS. non-cardiac myocytes (mainly cardiac fibroblasts) to adhere to the plastic after incubated for 1–2 h in a 100-mm dish. Then suspended cells (NRCMs) were collected and cultured.

2.7. Immunofluorescence

Immunofluorescence staining was performed as described in our previous study [25]. Cells were incubated with primary antibodies against VE-cadherin (Abcam, ab33168, diluted with 1:100) and vimentin (Santa Cruz, sc-5565, diluted with 1:50).

2.8. RT-PCR

RT-PCR and Western blotting were performed as described in our previous studies [21,23]. Total RNA was extracted from either frozen mouse cardiac tissue or cardiomyocytes using TRIzol. RNA (2 μg of each

Table 1
Primer sequences used for RT-PCR.

mRNA	Forward	Reverse
ANP[a]	ACCTGCTAGACCACCTGGAG	CCTTGGCTGTTATCTTCGGTACCGG
BNP[a]	GAGGTCACTCCTATCCTCTGG	GCCATTTCCTCCGACTTTTCTC
β-MHC[a]	CCGAGTCCCAGGTCAACAA	CTTCACGGGCACCCTTGGA
Col1agen I[a]	AGGCTTCAGTGGTTTGGATG	CACCAACAGCACCATCGTTA
Col1agen III[a]	AAGGCTGCAAGATGGATGCT	GTGCTTACGTGGGACAGTCA
CTGF[a]	AGGGCCTCTTCTGCGATTTC	CTTTGGAAGGACTCACCGCT
Fibronectin[a]	CCGGTGGCTGTCAGTCAGA	CCGTTCCCACTGCTGATTTATC
CTGF[a]	TGTGTGATGAGCCCAAGGAC	AGTTGGCTCGCATCATAGTTG
Sanil1[a]	CCAAACCCACTCGGATGTGA	TCTTGGTGCTTGTGGAGCAA
Snail2[a]	TTCTACGTTCTCTGGGCTGG	GCAGTGAGGGCAAGAGAAAG
Twist1[a]	TCGGACAAGCTGAGCAAGAT	CCAGACGGAGAAGGCGTAG
Twist2[a]	GCTACAGCAAGAAATCGAGCG	CTGCAGCTCCTCGAAAGACT
GAPDH[a]	ACTCCACTCACGGCAAATTC	TCTCCATGGTGGTGAAGACA
Collagen I[b]	GAGAGAGCATGACCGATGGATT	TGGACATTAGGCGCAGGAA
Collagen III[b]	ATAAGGGCAGGGAACAACTGAT	GTGAAGCAGGGTGAGAAGAAAC
CTGF[b]	GGAAGACACATTTGGCCCAG	GGCTTGGCGATTTTAGGTGT
GAPDH[b]	GACATGCCGCCTGGAGAAAC	AGCCCAGGATGCCCTTTAGT

Sequences are listed 5′–3′.
[a] The PCR used the primers in mice.
[b] The PCR used the primers in rat.

Table 2
List of abbreviations.

Abbreviation	Full name
AMPK	adenosine 5′-monophosphate (AMP)-activated protein kinase
BW	body weight
CSA	cross-section area
ECM	extracellular matrix
ECs	endothelial cells
EF	ejection fraction
EndMT	endothelial-to-mesenchymal transition
FBG	fasting blood glucose
FS	ejection shortening
HG	high glucose
HUVECs	human umbilical vein endothelial cells
HW	heart weight
LKB1	liver kinase B1
LV	left ventricular
MHECs	mouse heart endothelial cells
mTOR	mammalian target of rapamycin
STZ	streptozotocin
TGFβ	transforming growth factor beta
VE	vascular endothelial

sample) was reverse transcribed into cDNA using oligo (DT) primers and a Transcriptor First Strand cDNA Synthesis Kit We performed. PCR amplifications in all groups were quantified using a LightCycler 480 SYBR Green 1 Master Mix. 20 μl reactions according to the manufacturer's protocol with the following cycling parameters: 95 °C for 5 min; 45 cycles of 95 °C for 10 s, 60 °C for 10 s, and 72 °C for 10 s; 95 °C for 5 s; 60°Cfor 1 min; 97 °C for 0.11 s; and 40 °C for 10 min. The results were analyzed with the $2^{-\Delta\Delta Cq}$ method and normalized to GAPDH gene expression. Table 1 lists the primers used.

2.9. Western blot

Protein was extracted from cardiac tissue and cells. The cell lysate (50 μg) was fractionated by 10% sodium dodecyl sulfate-polyacrylamide gel electrophoresis (SDS-PAGE), subsequently transferred onto an Immobilon-P membrane using a gel transfer device (Invitrogen) and incubated with different primary antibodies, including: CD31, VE-cadherin, collagen I, collagen III, α-SMA, total AMPKa1, LKB1, and P-LKB1 (all purchased from Abcam, diluted with 1:1000), smad4, mTOR, and P-AMPKa1 (all purchased from Cell Signaling Technology, diluted with 1:1000). The following secondary antibody was used: goat anti-rabbit IgG or goat anti-mouse IgG (LI-COR), was for 60 min. The blots were scanned by a two-color infrared imaging system (Odyssey; LICOR) to quantify protein expression (Table 2).

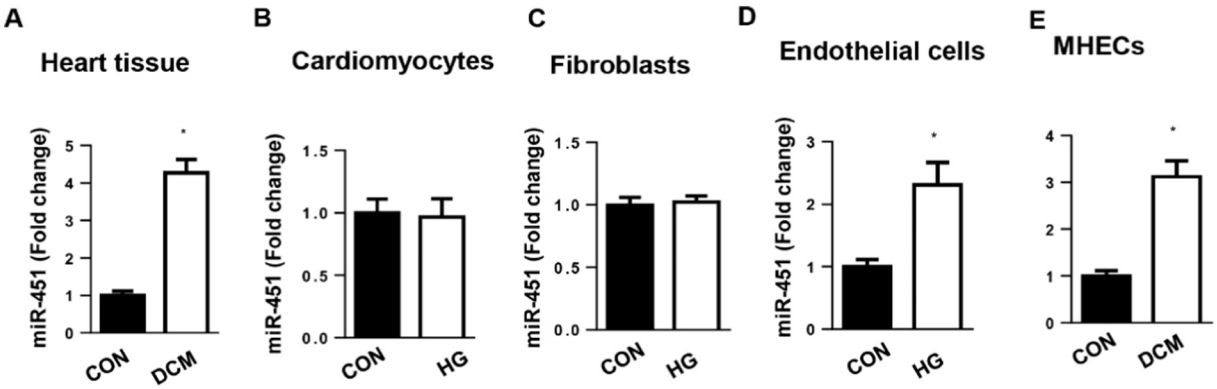

Fig. 1. The expression level of miR-451 in diabetic mouse heart.
A. The expression level of miR-451 in STZ-induced diabetic mouse heart (n = 6). B. The expression level of miR-451 in high glucose-stimulated cardiomyocytes (n = 6). C. The expression level of miR-451 in high glucose-stimulated fibroblasts (n = 6). D. The expression level of miR-451 in high glucose-stimulated endothelial cells (n = 6). E. The expression level of miR-451 in MHECs in diabetic mice heart (n = 6). *$P < 0.05$ vs. CON group.

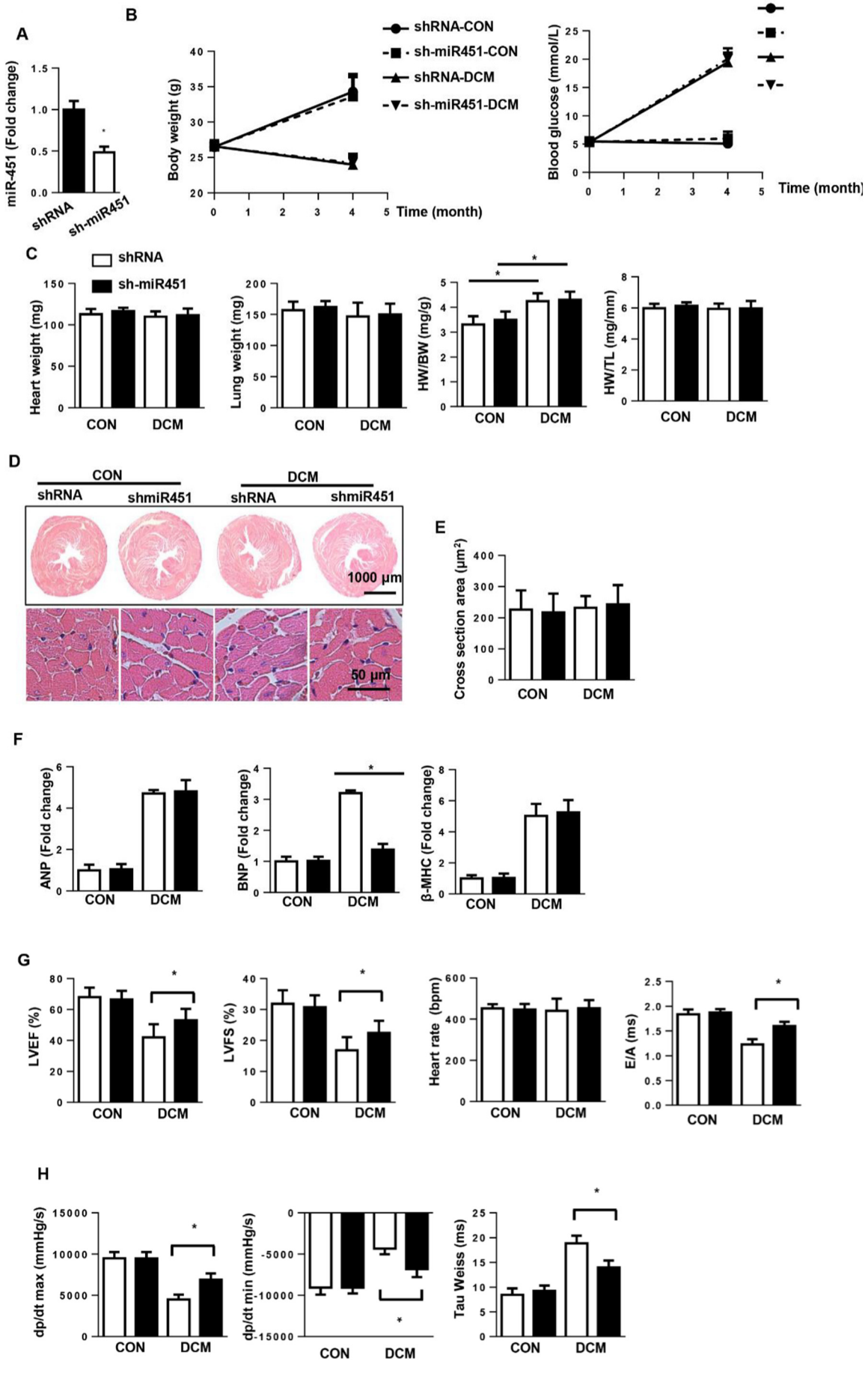

(caption on next page)

Fig. 2. MiR451 knockdown improves cardiac function in diabetic mice.
A. The expression level of miR-451 in mouse heart 4 weeks after Ad-shmiR451 injection (n = 6). *$P < 0.05$ vs. shRNA group. B. Body weight and blood glucose 0 and 4 months after STZ injection in the indicated groups (n = 12). C. Heart weight, lung weight, heart weight-to-body weight ratio (HW/BW), and heart weight-to-tibia length ratio (HW/TL) in DCM hearts in the indicated groups (n = 10). D. Representative image of the heart with H&E staining (n = 6). E. The cell surface area of cardiomyocytes in heart tissue (n = 100+ cells per group). F. PCR analyses of hypertrophic markers (ANP, BNP, β-MHC) in DCM mouse heart tissue (n = 6). G. Echocardiography measurement in DCM mouse hearts in the indicated group (n = 8). H. Hemodynamic measurements in DCM mouse hearts in the indicated group (n = 8). *$P < 0.05$.

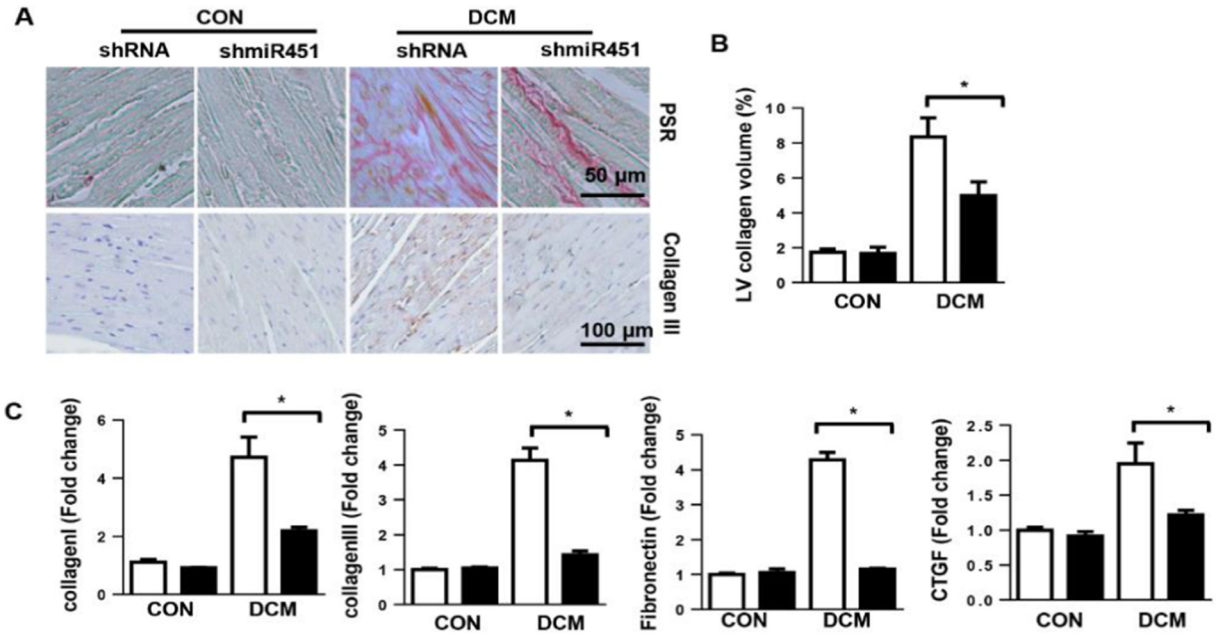

Fig. 3. MiR451 knockdown suppresses cardiac fibrosis in diabetic mice.
A. Representative image of the heart with picrosirius red (PSR) staining and immunohistochemical staining of collagen III (n = 6). B. Quantification of the total collagen volume in the indicated group. C. PCR analyses of fibrotic markers (collagen I, collagen III, TGFβ, and CTGF) in diabetic heart tissue (n = 6). *$P < 0.05$.

2.10. Statistical analysis

SPSS 23.0 was used for data analysis. The results are expressed as the means ± SD. Two-way analysis of variance (ANOVA) followed by the post hoc LSD test were used for comparisons within groups. Student's unpaired *t*-test was used for comparisons between two groups. All experiments were performed in a blinded manner. A P value < 0.05 was defined as statistically significant.

3. Results

3.1. The expression level of miR-451 in diabetic mice heart

We first detected the expression levels of miR-451 in diabetic mouse hearts and cells. As shown in Fig. 1, miR-451 levels were increased in STZ-induced DCM mouse heart but unchanged in high glucose-stimulated cardiomyocytes. We also detected the expression level of miR-451 in fibroblasts and endothelial cells (ECs). As a result, miR-451 levels only increased in ECs but were unchanged in fibroblasts. We also isolated the MHECs, and detected the miR-451 expression level in MHECs on diabetic heart. As shown in Fig. 1E, the expression level of miR-451 was up-regulated in MHECs in diabetic mice heart compared with that in control mice. These results suggest a functional role for miR-451 in ECs during the pathology of DCM.

3.2. MiR451 knockdown improves cardiac function in diabetic mice

To investigate the effect of miR-451 on cardiac dysfunction during diabetes pathology, mice were subjected to myocardial injections of Ad-shmiR-451 or Ad-shRNA to knock down miR-451 (Fig. 2A). Body weights increased in control mice and decreased in diabetic mice. Blood glucose increased in diabetic mice compared to the control group. Body weights and blood glucose were not significantly different between the shmiR451 mice and shRNA mice in both physical condition and diabetic status (Fig. 2B). Heart weights, lung weights, heart weight to tibia length ratio and the cross-sectional area (CSA) were not significantly different among the four groups (Fig. 2C–E). The heart weight-to-body weight ratio was increased in DCM mice compared with the control mice, but it was not significantly different between the shRNA-DCM group and shmiR-451-DCM group (Fig. 2C). The transcription levels of hypertrophic markers ANP, BNP and β-MHC increased in DCM mouse hearts compared with those in control mice. However, miR-451 knockdown did not affect the transcription levels of ANP and β-MHC but did affect the BNP level (Fig. 2F).

The echocardiography and hemodynamic results revealed that 4 months after STZ injection, systolic and diastolic dysfunction were observed in diabetic mice, as evidenced by an increased Tau value, reduced LVEF and LVFS, and decreased dp/dt_{max} and dp/dt_{min}. MiR451 knockdown did not affect heart rate in both physical condition and diabetic mice (Fig. 2G). MiR451 knockdown improved cardiac function (Fig. 2I). These data suggest that miR-451 participates in the progression of DCM.

3.3. MiR451 knockdown suppresses cardiac fibrosis in diabetic mice

Cardiac fibrosis was assessed using PSR staining and the transcription levels of fibrotic markers. Increased LV collagen volume and transcription levels of fibrotic markers were observed in diabetic mouse hearts (Fig. 3A–C). LV collagen volume and the transcription levels of fibrotic markers were reduced in miR451-silenced diabetic mice

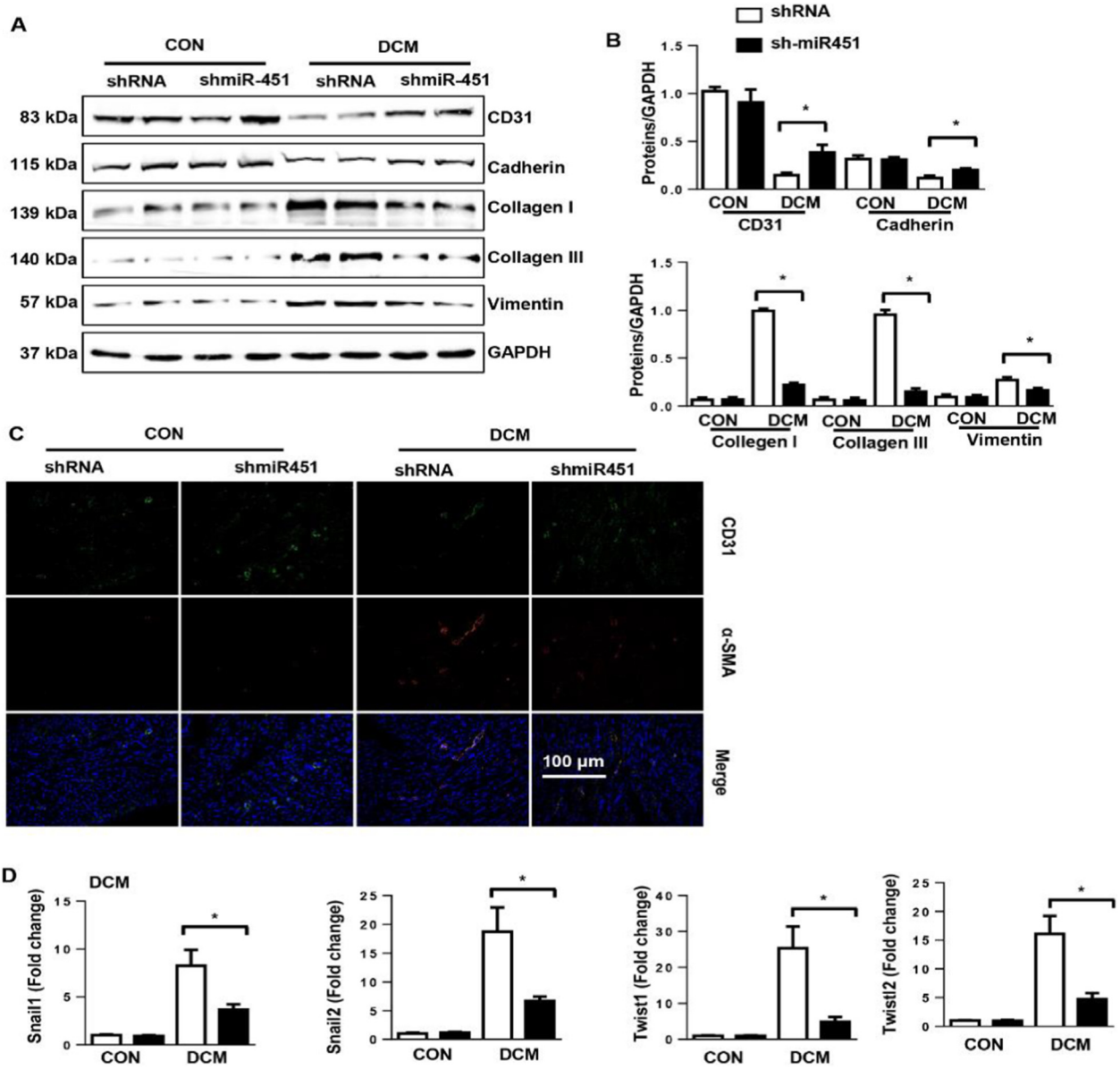

Fig. 4. MiR451 knockdown decreases EndMT in diabetic mice.
A and B. Representative Western blot (A) and analyses (B) of CD31, VE-cadherin, collagen I, collagen III, and vimentin in DCM mouse hearts (n = 6). C. Immunofluorescence staining of CD31 and α-SMA in diabetic hearts (n = 6). D. PCR analysis of EndMT markers (snial1, snial2, twist1, and twist2) in DCM mouse heart tissue (n = 6). $^{*}P < 0.05$.

(Fig. 3A–C).

3.4. MiR451 knockdown decreases EndMT in diabetic mice

Previous studies have proven that EndMT is involved in the pathology of cardiac fibrosis in both type 1 and type 2 diabetes-induced cardiomyopathy [7,8]. Since the expression level of miR-451 was altered in ECs during DCM, we investigated the role of miR-451 in EndMT. Increased expression levels of fibroblast markers (collagen I, collagen III, and vimentin) and decreased expression levels of endothelial markers (CD31 and cadherin) were observed in DCM mouse hearts compared with control mouse hearts (Fig. 4A–B). These expression alteration was also confirmed by immunofluorescence staining of CD31 and α-SMA with decreased expression of CD31 (green) and increased expression of α-SMA (Red) in DCM mouse hearts compared with control mouse hearts (Fig. 4C). The transcription levels of EndMT markers (snial1, snial2, twist1, and twist2) also increased in diabetic mice (Fig. 4D). MiR451 silencing reduced these EndMT transition phenotypes (Fig. 4A–D).

3.5. MiR451 antagomir attenuates high glucose-induced EndMT in MHECs

To confirm the direct effect of miR-451 on ECs, MHECs were isolated and cultured with high glucose in the presence of a miR-451 antagomir for 48 h. HG stimulation decreased cell viability, while miR-451 antagomir increased cell viability (Fig. 5A). HG increased EndMT in MHECs as assessed by immunofluorescence staining results with a decreased expression of VE-cadherin (green) and increased expression of vimentin (Red) in HG stimulated ECs compared with control ECs (Fig. 5B). These alterations were also confirmed by Western blot results with increased expression levels of fibrotic markers (α-SMA and vimentin) and decreased expression levels of endothelial markers (CA31 and VE-cadherin) (Fig. 5C–D). The miR-451 antagomir reduced these transitions (Fig. 5B–D). The miR-451 antagomir reduced the increased

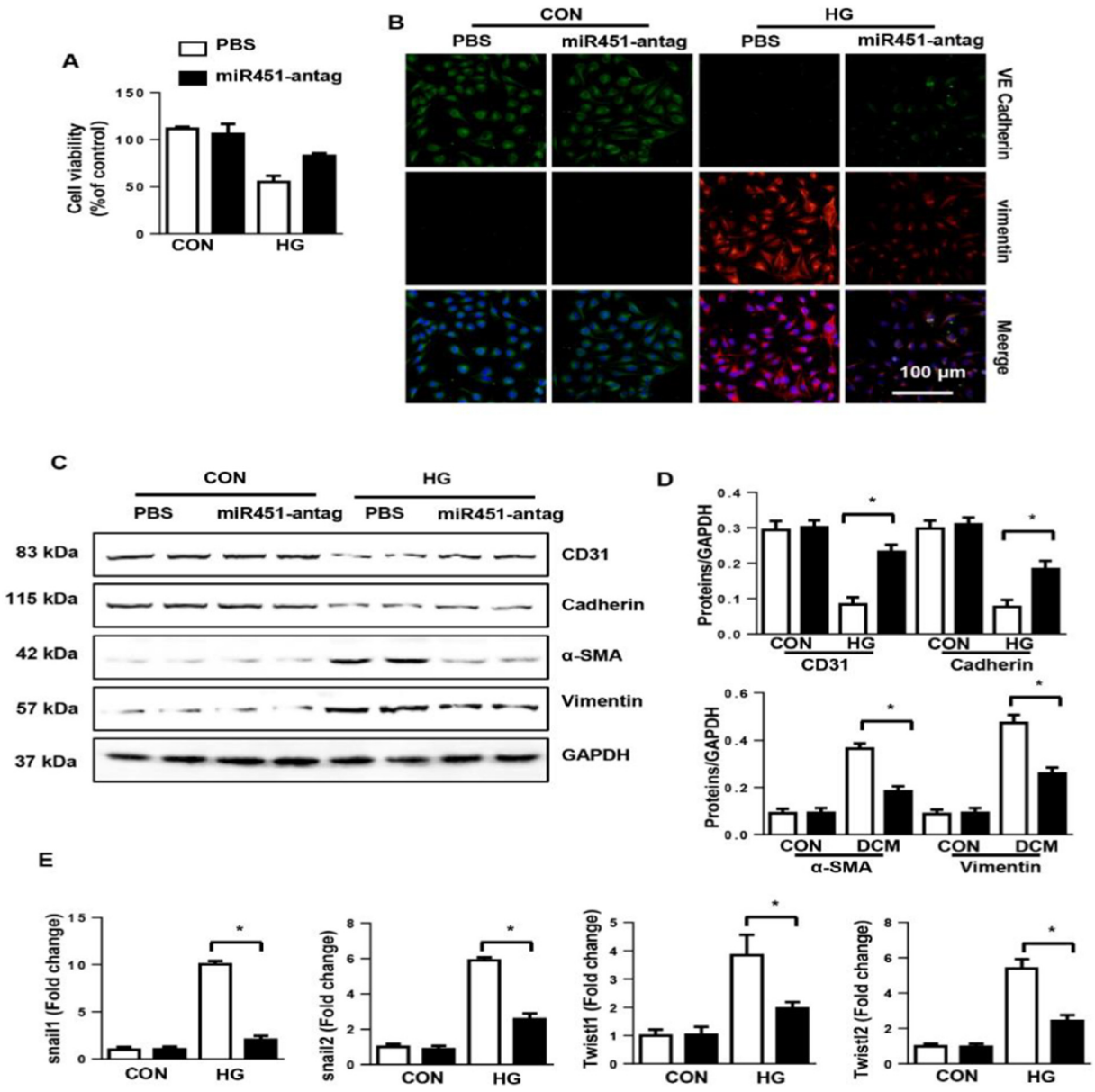

Fig. 5. MiR-451 antagomir attenuates high glucose-induced EndMT in MHECs
A. Cell viability in MHECs treated with miR-451 antagomir under HG condition (n = 6 samples). B. Immunofluorescence staining of VE-cadherin and vimentin in MHECs (n = 6 samples). C and D. Representative Western blot (C) and analyses (D) of CD31, VE-cadherin, α-SMA, and vimentin after cells were treated with a miR-451 antagomir and exposed to HG (n = 6 samples). E. PCR analyses of EndMT markers (snial1, snial2, twist1, and twist2) in MHECs (n = 6 samples). $^{*}P < 0.05$.

transcription levels of EndMT markers (snail1, snail2, twist1, and twist2) (Fig. 5E).

3.6. The effects of miR-451 on AMPKa1 signaling

Our previous study reported that miR-451 inhibited AMPKa signaling in cardiomyocytes. Thus, we measured AMPKa1 signaling in MHECs. Consistent with our previous study, we found that AMPKa1 was inactivated, and the phosphorylation levels of the downstream protein mTOR were increased in both diabetic mouse hearts and HG-stimulated MHECs. The miR-451 antagomir increased the phosphorylation levels of AMPKa1 and reduced the phosphorylation levels of mTOR in diabetic mouse hearts (Fig. 6A, B) and HG-stimulated MHECs (Fig. 6C, D). We also detected the effect of miR-451 on AMPKα2, as shown in Fig. 6A and C, the expression level of p-AMPKα2 was decreased in both DCM mice heart and HG stimulated ECs, but both miR-451 knockdown and antagonism did not affect the phosphorylated AMPKα2 level.

3.7. AMPKa1 silencing offsets the effects of the miR-451 antagomir

To confirm whether AMPKa1 activation mediated the protective effects of miR-451 antagomir, cells were treated with AMPKa1 siRNA to knock down AMPKa1 (Fig. 7A). Increased smad4 activation was observed in cells treated with AMPKa1 siRNA (Fig. 7B, C). The EndMT levels in cells treated with AMPKa1 siRNA were not significantly different than in the HG group as evidenced by the same level of VE-cadherin and vimentin expression in both Western blot result (Fig. 7B, C) and immunofluorescence result (Fig. 7D), and the same extent of transcription of EndMT markers (Fig. 7E). The miR-451 antagomir did not reverse the increase in EndMT in cells treated with AMPKa1 siRNA as assessed by the same expression level of VE-cadherin and vimentin and transcription level of EndMT markers between ECs treated with siAMPKα and ECs treated with siAMPKα and miR-451 antagomir

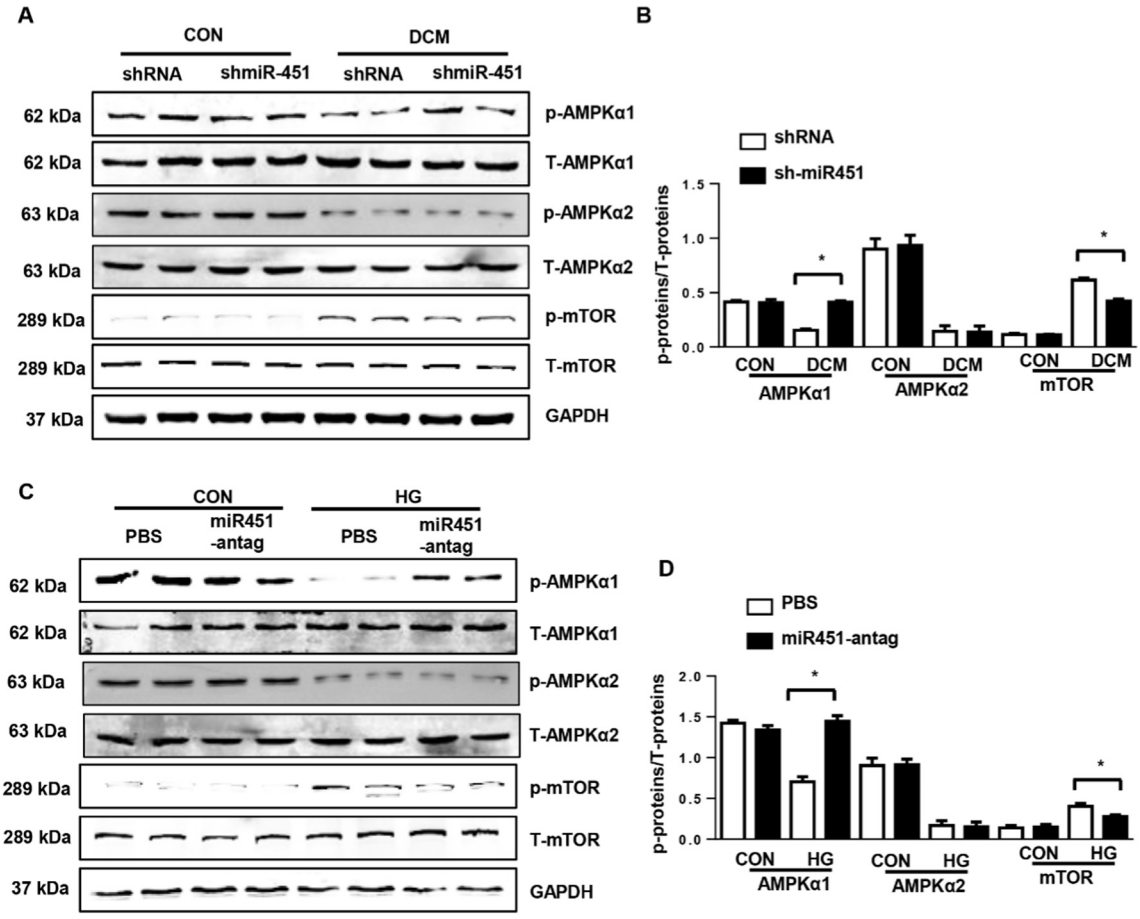

Fig. 6. The effects of miR-451 on AMPKa signaling.
A and B. Representative Western blot (A) and analyses (B) of P-AMPKa1, T-AMPKa1, P-AMPKa2, T-AMPKa1, P-mTOR, and T-mTOR in DCM mouse heart in the indicated group (n = 6). C and D. Representative Western blot (C) and analyses (D) of P-AMPKa1, T-AMPKa1, P-AMPKa2, T-AMPKa1, P-mTOR, and T-mTOR in MHECs treated with miR-451 antagomir (n = 6 samples). $^*P < 0.05$.

(Fig. 7B–E). These results indicate that AMPKa knockdown abrogates the anti-EndMT effects of the miR-451 antagomir. Altogether, these data suggest that miR-451 affects EndMT via regulation of AMPKa1/smad signaling.

3.8. miR-451 targets Cab39/LKB1 to regulate AMPKa1 signaling

A previous study reported that calcium-binding protein 39 (Cab39), which is an obligatory co-factor for the serine/threonine kinase LKB1, was a direct target of miR-451 in cardiomyocytes [20]. We examined whether miR-451 targets Cab39/LKB1 to regulate AMPKa1 signaling. As shown in Fig. 8, LKB1 activation was downregulated in HG-stimulated MHECs and increased in miR-451 antagomir-treated MHECs. Consistent with LKB1, Cab39 was downregulated in HG-stimulated MHECs and increased in miR-451 antagomir-treated MHECs. These results suggest that by targeting Cab39/LKB1, miR-451 regulates AMPKa1 signaling in ECs. To evaluate whether miR-451 effect on CFs, CFs were treated with TGFβ1 and a miR-451 antagomir. As shown in Fig. 8C and D, TGFβ1 increased CF activation and collagen expression, and the miR-451 antagomir attenuated CF activation and collagen expression.

4. Discussion

MiRNAs are small (20–25-nucleotide) RNA molecules that affect gene expression. The precursor molecules of miRNAs (pre-miRNAs) are derived by RNA polymerase II as long fragments in the nucleus. After being processed by different molecular machineries, they form mature double-stranded miRNAs that bind with target genes and silence gene activity at the posttranscriptional level [26]. Many studies have revealed that miRNA expression is highly altered in various cardiovascular issues, and these alterations are associated with cell growth, survival, and death [27] [20]. In our study, we found that miR-451 was upregulated in DCM mouse hearts but not in HG-stimulated cardiomyocytes or fibroblasts. MiR-451 was upregulated in HG-stimulated ECs, which supports a role of miR-451 in ECs. The mechanism of glucose increase miR-451 expression may attribute to the reduced expression of upstream LncRNA. Further study are needed to confirm the specific mechanism that glucose increase miR-451. Sixteen weeks after STZ injection, mice exhibited cardiac dysfunction and remarkable cardiac fibrosis. MiR-451 knockdown improved cardiac dysfunction and suppressed cardiac fibrosis. We did not observed cardiac hypertrophy although the HW/BW was increased in the DCM group, both heart weight and HW/TL value were unchanged between control mice and DCM mice. Since the body weight was significantly reduced in DCM mice, the increased HW/BW in DCM group may attribute the decreased body weight other than the increased heart weight. This result was much consistent with a previous study that they also did not observed increased heart weight during STZ induced diabetic cardiomyopathy mice model [28].

Evidence implicating EndMT in cardiac fibrosis has been mounting for several years. In a landmark publication in 2007, Kalluri et al. demonstrated that EndMT significantly contributed to myocardial fibrosis (27%–33%) in the adult heart [6]. Then, EndMT/EMT was proven to be

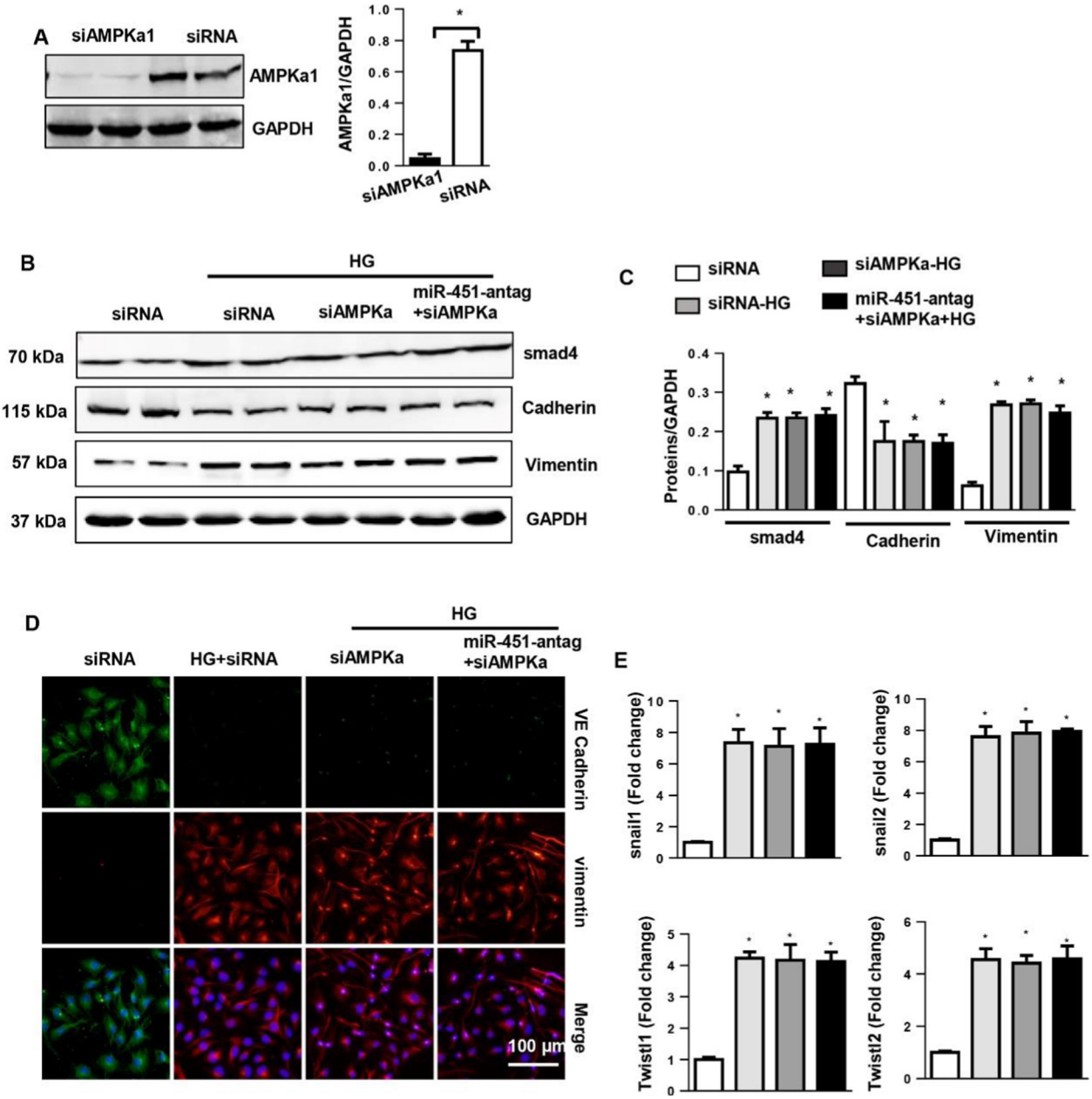

Fig. 7. AMPKa1 silencing offsets the effects of the miR-451 antagomir.
A–E. MHECs were treated with a miR-451 antagomir and AMPKa1 siRNA and exposed to HG. A. The expression of AMPKa1 after cells were treated with siRNA (n = 6 samples). B and C. The expression level of VE-cadherin and vimentin in the indicated group (n = 6 samples). D. Immunofluorescence staining of VE-cadherin and vimentin in the indicated group (n = 6 samples). E. PCR analyses of EndMT markers (snial1, snial2, twist1, and twist2) in MHECs (n = 6 samples). *$P < 0.05$ vs. the siRNA group.

associated with cardiac fibrosis in many other cardiovascular disease models such as hypertrophic cardiomyopathy and diabetes-induced heart disease [7]. During the pathology of diabetes, ECs are one of the earliest cell types exposed to hyperglycemia [8]. Hyperglycemia is also associated with metabolic abnormalities, which lead to EC damage and change. This damage leads to a complex network of gene activation and repression programs. During these processes, ECs change their polarity, morphology, functionality and cell-cell interaction to adopt a mesenchymal phenotype [11]. Previous studies demonstrated the benefit of inhibiting EndMT in DCM [7,8]. In the current study, we show that diabetes-induced EndMT increased with increased fibrosis level. EndMT was also observed in high glucose-stimulated MHECs. MiR-451 knockdown and an antagomir inhibited these phenotypic changes in endothelial cells and prevented diabetes-induced cardiac functional abnormalities.

AMPK is a serine-threonine kinase that acts as a fuel gauge in the process of cell stress to maintain energy balance [29]. AMPK functions in diabetes, cancer and cardiovascular disease [29]. Vascular AMPK guarantees an energy supply to modulate vascular function and blood flow under physiological conditions [30]. However, when ECs expose to sustained hyperglycemia, vascular AMPK undergoes chronic deactivation, which shifts the balance to metabolic disorder and leads to EC damage [8]. Recent studies have reported that AMPK activation inhibited the TGFβ pathway. Zheng W reported that the AMPK agonist metformin prevents peritendinous fibrosis via inhibition of TGFβ signaling [31]. Xiao Y found that AMPK activation inhibited the TGF-β/smad pathway, which mediated the protective effect of baicalin on pressure overload-induced cardiac fibrosis [32]. Moreover, Hinson JT

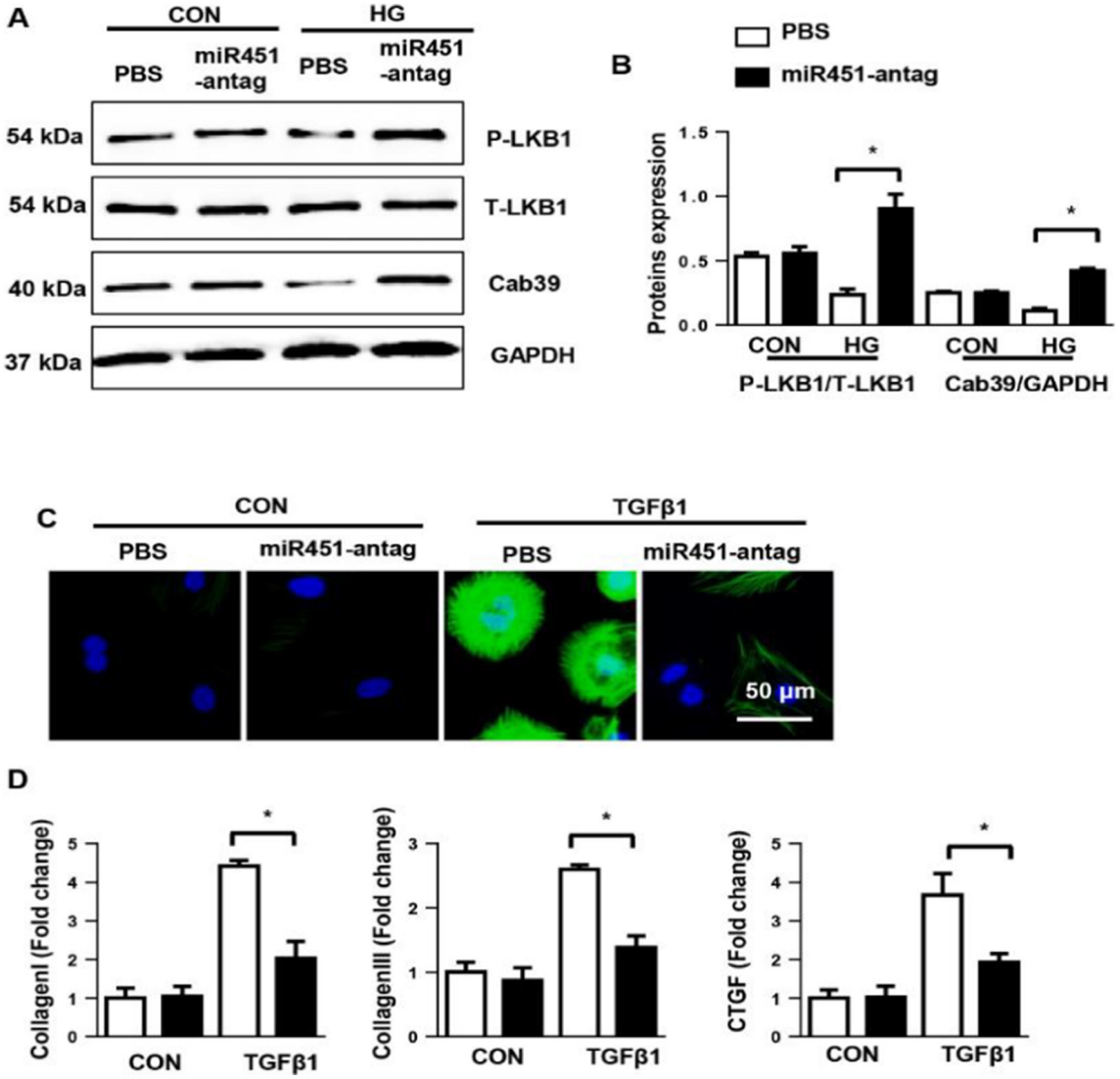

Fig. 8. miR-451 targets Cab39/LKB1 to regulate AMPKa1 signaling.
A and B. Representative Western blot (A) and analyses (B) of P-LKB1, T-LKB1, and Cab39 in MHECs treated with a miR-451 antagomir (n = 6 samples). *$P < 0.05$. C and D. CFs were treated with TGFβ1 and a miR-451 antagomir for 24 h. C. Immunofluorescence staining of αmSMA in the indicated group (n = 6 samples). D. PCR analyses of fibrosis markers (collagen I, collagen III, and CTGF) in CFs (n = 6 samples). *$P < 0.05$.

found a crosstalk between AMPK and the posttranscriptional regulation of TGFβ signaling that was implicated in fibrotic forms of cardiomyopathy [33]. In cardiomyocytes, miR-451 targets Cab39, a scaffold protein of LKB1, thus inhibiting AMPK activation and exertion [20]. In our study, we found that the effects of miR-451 on EndMT were dependent on AMPKa activation in MHECs via Cab39/LKB1. Considering that endothelial cells express both α1 and α2 subunits and that AMPKα1 is predominant in ECs, we silenced the AMPKα1 subunits with AMPKα1 siRNA. AMPKa1 knockdown increased smad4 activation, which completely abolished the anti-EndMT effects of the miR-451 antagomir. These results suggest that the miR-451 antagomir inhibits smad signaling via AMPKa1 activation to exert its anti-EndMT and cardioprotective effects in DCM.

CF activation is an essential process during cardiac fibrosis. We measured the effects of miR-451 on CFs. We found that the miR-451 antagomir attenuated CF activation and collagen expression. These results suggest that the miR-451 antagomir targets ECs and CFs to exert anti-fibrosis effects during DCM pathology.

5. Conclusion

In summary, we found that miR-451 participated in cardiac fibrosis during DCM pathology via regulation of EndMT in ECs and CFs activation. Our study supports miR-451 as a promising target for the treatment of DCM.

Competing interests

The authors declare no conflicts of interest.

Grant sponsor

This study was supported by the Medical Science and Technology Research Project of Henan province (Grant No. 201702063).

Authors' contributions

Cui Liang and Yanzhou Zhang contributed to the conception and design of the experiments. Lu Gao, Yuan Liu, Yuzhou Liu, and Rui Yao performed the experiments. Yapeng Li, Lili Xiao analyzed the

experimental results. LeimingWu, BinbinDu and Zhen Huang wrote and revised the manuscript.

Acknowledgments

Not applicable.

References

[1] N. Alonso, P. Moliner, D. Mauricio, Pathogenesis, clinical features and treatment of diabetic cardiomyopathy, Adv. Exp. Med. Biol. 1067 (2018) 197–217.
[2] I. Russo, N.G. Frangogiannis, Diabetes-associated cardiac fibrosis: cellular effectors, molecular mechanisms and therapeutic opportunities, J. Mol. Cell. Cardiol. 90 (2016) 84–93.
[3] Kawaguchi, M., Techigawara, M., Ishihata, T., Asakura, T., Saito, F., Maehara, K. Maruyama, Y., A comparison of ultrastructural changes on endomyocardial biopsy specimens obtained from patients with diabetes mellitus with and without hypertension, Heart Vessel.. 12(6)(1997) 267–74.
[4] S. Chen, T. Evans, K. Mukherjee, M. Karmazyn, S. Chakrabarti, Diabetes-induced myocardial structural changes: role of endothelin-1 and its receptors, J. Mol. Cell. Cardiol. 32 (9) (2000) 1621–1629.
[5] D. Hileeto, M. Cukiernik, S. Mukherjee, T. Evans, Y. Barbin, D. Downey, M. Karmazyn, S. Chakrabarti, Contributions of endothelin-1 and sodium hydrogen exchanger-1 in the diabetic myocardium, Diabetes Metab. Res. Rev. 18 (5) (2002) 386–394.
[6] Zeisberg, E.M., Tarnavski, O., Zeisberg, M., Dorfman, A.L., McMullen, J.R., Gustafsson, E., Chandraker, A., Yuan, X., Pu, W.T., Roberts, A.B., Neilson, E.G., Sayegh, M.H., Izumo, S. Kalluri, R., Endothelial-to-mesenchymal transition contributes to cardiac fibrosis, Nat. Med.. 13(8)(2007) 952–61.
[7] X. Liu, H. Mujahid, B. Rong, Q.H. Lu, W. Zhang, P. Li, N. Li, E.S. Liang, Q. Wang, D.Q. Tang, N.L. Li, X.P. Ji, Y.G. Chen, Y.X. Zhao, M.X. Zhang, Irisin inhibits high glucose-induced endothelial-to-mesenchymal transition and exerts a dose-dependent bidirectional effect on diabetic cardiomyopathy, J. Cell. Mol. Med. 22 (2) (2018) 808–822.
[8] Feng, B., Cao, Y., Chen, S., Chu, X., Chu, Y. Chakrabarti, S., miR-200b mediates endothelial-to-mesenchymal transition in diabetic cardiomyopathy, Diabetes. 65(3) (2016) 768–79.
[9] Y. Yue, K. Meng, Y. Pu, X. Zhang, Transforming growth factor beta (TGF-beta) mediates cardiac fibrosis and induces diabetic cardiomyopathy, Diabetes Res. Clin. Pract. 133 (2017) 124–130.
[10] J.K. Lighthouse, E.M. Small, Transcriptional control of cardiac fibroblast plasticity, J. Mol. Cell. Cardiol. 91 (2016) 52–60.
[11] L. Xiao, A.C. Dudley, Fine-tuning vascular fate during endothelial-mesenchymal transition, J. Pathol. 241 (1) (2017) 25–35.
[12] Z. Li, T.M. Rana, Therapeutic targeting of microRNAs: current status and future challenges, Nat. Rev. Drug Discov. 13 (8) (2014) 622–638.
[13] F. Yi, Y. Shang, B. Li, S. Dai, W. Wu, L. Cheng, X. Wang, MicroRNA-193-5p modulates angiogenesis through IGF2 in type 2 diabetic cardiomyopathy, Biochem. Biophys. Res. Commun. 491 (2017) 876–882.
[14] X. Liu, Shixue Liu, Role of microRNAs in the pathogenesis of diabetic cardiomyopathy, Biomed Rep 6 (2) (2017) 140–145.
[15] H. Gal, G. Pandi, A.A. Kanner, Z. Ram, G. Lithwick-Yanai, N. Amariglio, G. Rechavi, D. Givol, MIR-451 and Imatinib mesylate inhibit tumor growth of glioblastoma stem cells, Biochem. Biophys. Res. Commun. 376 (1) (2008) 86–90.
[16] D.Q. Chen, C. Yu, X.F. Zhang, Z.F. Liu, R. Wang, M. Jiang, H. Chen, F. Yan, M. Tao, L.B. Chen, H. Zhu, J.F. Feng, HDAC3-mediated silencing of miR-451 decreases chemosensitivity of patients with metastatic castration-resistant prostate cancer by targeting NEDD9, Ther Adv Med Oncol 10 (2018) (1758835918783132).
[17] Liu, K., Tian, H., Zhang, Y., Zhao, H. Ma, K., miR-451 selectively increases sensitivity to cisplatin in ERCC1-high non-small cell lung cancer cells, J. Cell. Biochem.. 2018).
[18] Sun Y, P.R., Peng H, Liu H, Wen L, Wu T, Yi H, Li A, Zhang Z, miR-451 suppresses the NF-kappaB-mediated proinflammatory molecules expression through inhibiting LMP7 in diabetic nephropathy, Mol. Cell. Endocrinol.. 433 2016) 75–86.
[19] L. Song, Ming Su, S. Wang, Y. Zou, X. Wang, Y. Wang, H. Cui, P. Zhao, R. Hui, J. Wang, MiR-451 is decreased in hypertrophic cardiomyopathy and regulates autophagy by targeting TSC1, J. Cell. Mol. Med. 18 (11) (2014) 2266–2274.
[20] Y. Kuwabara, T. H., O. Baba, S. Watanabe, M. Nishiga, S. Usami, M. Izuhara, T. Nakao, T. Nishino, K. Otsu, T. Kita, T. Kimura, K. Ono, MicroRNA-451 exacerbates lipotoxicity in cardiac myocytes and high-fat diet-induced cardiac hypertrophy in mice through suppression of the LKB1/AMPK pathway, Circ. Res. 116 (2) (2015) 279–288.
[21] Y. Xiao, Q.Q. Wu, M.X. Duan, C. Liu, Y. Yuan, Z. Yang, H.H. Liao, D. Fan, Q.Z. Tang, TAX1BP1 overexpression attenuates cardiac dysfunction and remodeling in STZ-induced diabetic cardiomyopathy in mice by regulating autophagy, Biochim. Biophys. Acta 1864 (5) (2018) 1728–1743 Pt A.
[22] Q.Q. Wu, Y. Yuan, X.H. Jiang, Y. Xiao, Z. Yang, Z.G. Ma, H.H. Liao, Y. Liu, W. Chang, Z.Y. Bian, Q.Z. Tang, OX40 regulates pressure overload-induced cardiac hypertrophy and remodelling via CD4+ T-cells, Clin Sci (Lond) 130 (22) (2016) 2061–2071.
[23] Y. Xiao, Z. Yang, Q.Q. Wu, X.H. Jiang, Y. Yuan, W. Chang, Z.Y. Bian, J.X. Zhu, Q.Z. Tang, Cucurbitacin B protects against pressure overload induced cardiac hypertrophy, J. Cell. Biochem. 118 (11) (2017) 3899–3910.
[24] Q.Q. Wu, M. Xu, Y. Yuan, F.F. Li, Z. Yang, Y. Liu, M.Q. Zhou, Z.Y. Bian, W. Deng, L. Gao, H. Li, Q.Z. Tang, Cathepsin B deficiency attenuates cardiac remodeling in response to pressure overload via TNF-alpha/ASK1/JNK pathway, Am. J. Physiol. Heart Circ. Physiol. 308 (9) (2015) H1143–H1154.
[25] Q.Q. Wu, Y. Xiao, X.H. Jiang, Y. Yuan, Z. Yang, W. Chang, Z.Y. Bian, Q.Z. Tang, Evodiamine attenuates TGF-beta1-induced fibroblast activation and endothelial to mesenchymal transition, Mol. Cell. Biochem. 430 (1–2) (2017) 81–90.
[26] N. Ghosh, R. Katare, Molecular mechanism of diabetic cardiomyopathy and modulation of microRNA function by synthetic oligonucleotides, Cardiovasc. Diabetol. 17 (1) (2018) 43.
[27] C.P.M. Chen, C. Liu, J. Gao, K. Wang, P. Li, MicroRNA as a therapeutic target in cardiac remodeling, Biomed. Res. Int. 2017 (2017) 1278436,3.
[28] N. Zhang, Z. Yang, S.Z. Xiang, Y.G. Jin, W.Y. Wei, Z.Y. Bian, W. Deng, Q.Z. Tang, Nobiletin attenuates cardiac dysfunction, oxidative stress, and inflammatory in streptozotocin: induced diabetic cardiomyopathy, Mol. Cell. Biochem. 417 (1–2) (2016) 87–96.
[29] Y. Feng, Y. Zhang, H. Xiao, AMPK and cardiac remodelling, Sci. China Life Sci. 61 (1) (2018) 14–23.
[30] B. Fisslthaler, I. Fleming, Activation and signaling by the AMP-activated protein kinase in endothelial cells, Circ. Res. 105 (2) (2009) 114–127.
[31] W. Zheng, J. Song, Y. Zhang, S. Chen, H. Ruan, C. Fan, Metformin prevents peritendinous fibrosis by inhibiting transforming growth factor-beta signaling, Oncotarget 8 (60) (2017) 101784–101794.
[32] Y. Xiao, J. Ye, Y. Zhou, J. Huang, X. Liu, B. Huang, L. Zhu, B. Wu, G. Zhang, Y. Cai, Baicalin inhibits pressure overload-induced cardiac fibrosis through regulating AMPK/TGF-beta/Smads signaling pathway, Arch. Biochem. Biophys. 640 (2018) 37–46.
[33] J.T. Hinson, A. Chopra, A. Lowe, C.C. Sheng, R.M. Gupta, R. Kuppusamy, J. O'Sullivan, G. Rowe, H. Wakimoto, J. Gorham, M.A. Burke, K. Zhang, K. Musunuru, R.E. Gerszten, S.M. Wu, C.S. Chen, J.G. Seidman, C.E. Seidman, Integrative analysis of PRKAG2 cardiomyopathy iPS and microtissue models identifies AMPK as a regulator of metabolism, survival, and fibrosis, Cell Rep. 17 (12) (2016) 3292–3304.